International Journal of Mathematics and Computational Science
Vol. 4, No. 3, 2018, pp. 86-98
http://www.aiscience.org/journal/ijmcs
ISSN: 2381-7011 (Print); ISSN: 2381-702X (Online)

Heat and Mass Transfer of a Maxwell Nanofluid over a Stretching Surface with Variable Thickness Embedded in Porous Medium

Elsayed Mohamed Abdel Rahman Elbashbeshy[1], Khaled Mohamed Abdelgaber[2], Hamada Galal Asker[2, *]

[1]Mathematics Department, Faculty of Science, Ain Shams University, Abbassia, Cairo, Egypt
[2]Department of Physics & Engineering Mathematics, Faculty of Engineering, Mataria, Helwan University, Cairo, Egypt

Abstract

In the presence of a heat source, heat and mass transfer of the flow of a Maxwell nanofluid over a stretching surface with variable thickness embedded in a porous medium is investigated. The governing equations are reduced to nonlinear ordinary differential equations by using similarity transformations. These equations are then solved numerically by Rung-Kutta fourth/fifth order method coupled with shooting technique. The results for the local skin friction, Nusselt number, and Sherwood number are presented and discussed graphically. The effects of variable thickness, heat source, and medium porosity on the dimensionless velocity, temperature, and concentration of the nanofluid are analyzed graphically. Results are compared with earlier published results under special cases.

Keywords

Maxwell Fluid, Stretching Surface, Variable Thickness, Nanofluid, Porous Medium, Heat Generation/Absorption Source

Received: April 19, 2018 / Accepted: May 17, 2018 / Published online: June 14, 2018

1. Introduction

The nanofluids are used to enhance the thermal conductivity of the conductive fluids such as the water. These nanofluids have several engineering applications such as in heat exchangers. The effectiveness of the heat exchangers is improved with the transmission fluids of high thermal conductivity. These nanofluids are formed by adding high thermal conductivity nanoparticles such as metals and nitrides. The nanoparticle diameter ranges between 1-100 nm. The major disadvantage of using the nanoparticles is the accumulation of dust in the pipes of the heat exchanger. However, the use of nanofluids is more reliable for the outside flow such as a stretching surface in the stationary fluid than the inside flow such as the flow in pipes.

Xuan and Qiang [1] succeeded in enhancing the thermal conductivity of some liquids by adding suspended copper nanophase powders. The suspended nanoparticles increase the surface area and the heat capacity. Also, it flattens the transverse temperature gradient. Therefore, the effective thermal conductivity of the fluid is enhanced. Daungthongsuk and Wongwises [2] summarized the researches concerning the forced heat transfer of the nanofluids ensuring the efficiency of using nanofluids. Hamilton and Crosser [3] established a mathematical model for predicting the thermal conductivity of homogeneous two-component mixtures. Stephen and Eastman [4] presented a theoretical study for suspended metallic nanoparticles in conventional heat transfer fluids using Hamilton and Crosser model. The model enhanced the thermal conductivity which in turn reduces the heat exchanger pumping power. Eastman

* Corresponding author
E-mail address: Asker_hamada@yahoo.com (H. G. Asker)

et al. [5] studied the effectiveness of adding copper nanometer-sized particles into ethylene glycol. The effective thermal conductivity was raised up to 40% over the base fluid. Also, the study indicated that there is no effect of either particle size or particle thermal conductivity of the mixture. Xie et al. [6] used suspensions containing nanometer-sized Alumina particles. Wang et al. [7] presented a fractal model to study the effective thermal conductivity of nanofluid considering its size and surface adsorption.

Wen and Ding [8] presented a practical survey for the effective thermal conductivity of aqueous suspensions of multiwall carbon nanotubes. Hong et al. [9] discussed the enhanced thermal conductivity of Fe-nanofluid. Buongiorno [10] introduced seven slip mechanisms to produce a relative velocity between the nanoparticles and the base fluid. Among of these mechanisms, the Brownian diffusion and the thermophoresis are important. Makinde and Aziz [11] surveyed the effects of Brownian motion and thermophoresis on the boundary layer flow in a nanofluid due to a linearly stretching surface. Sulochana and Sandeep [12] studied the effect of porosity on the flow of nanofluid over a stretching sheet for no slip and Navier slip conditions. Mabood et al. [13] studied numerically the effects of magnetic field and viscous dissipation for electrically conducting water-based nanofluid over a nonlinearly stretching surface and found a decrease in the velocity and increase in the temperature with the magnetic field. Elbashbeshy et al. [14] presented two slip effects, Brownian diffusion, and thermophoresis on flow, heat, and mass transfer of an incompressible nanofluid over a stretching horizontal cylinder in the presence of suction/injection. Furthermore, Elbashbeshy et al. [15] studied the unsteady flow of Maxwell fluid showing that the modified skin friction increases with the elasticity parameter, magnetic field, and material parameter. Sandeep et al. [16] analyzed the unsteady MHD radiative flow of dusty nanofluid over an exponentially permeable stretching surface. Pal and Mandal [17] studied the stagnation point flow over stretching/shrinking sheet of nanofluid with viscous-ohmic dissipation and thermal radiation.

The non-Newtonian Maxwell fluids over a stretching surface have appeared in the nanofluid researchers. Sadeghy and Sharifi [18] studied the boundary layer flow of Maxwell fluid over a flat stretching surface with local similarity solution. The study showed that the boundary layer thickness and the wall skin friction coefficient are increased for the fluid with higher elasticity. Alikabar et al. [19] studied numerically the influence of the thermal radiation on the MHD flow of Maxwell fluid above stretching sheet. The unsteady flow of the Maxwell fluid is discussed [20-26]. Sajid et al. [20] studied the flow of a second grade over a stretching sheet while Hayat and Qasim [21] presented the effects of the thermal radiation and Joule heating on the MHD flow of a Maxwell fluid in the presence of thermophoresis. Swati [22] studied the presence of a heat source/sink. The fluid velocity is decreased by increasing the magnetic parameter while the Maxwell parameter increases the velocity and the temperature fields.

Sawti et al. [23] discussed the effect of the thermal radiation and Swati and Bhattacharyya [24] presented a numerical solution for the unsteady flow in the presence of chemical reaction. Ramesh and Gireesha [25] studied the influence of heat source/sink on a Maxwell fluid over a stretching surface with a constant thickness in the presence of nanoparticles. Madhua et al. [26] studied the effects of the magnetic field and the thermal radiation. Hsiao [27] used the improved parameters control method to investigate the effects of the electrical MHD ohmic dissipation forced and free convection on the Maxwell fluid with a stagnation point. The study created an applicable model in manufacturing processes. Furthermore, Hsiao [28] extended the previous study for a viscoelastic non-Newtonian Carreau-nanofluid on a stagnation point.

The effectiveness of the surface thickness is introduced by Ramesh et al. [29] while studying the stagnation point flow over Casson fluid to show the effects of the variable thickness and thermal radiation. Khader and Magahed [30] introduced the effect of slip velocity for boundary layer flow due to a nonlinearly stretching sheet with variable thickness. Also, Fang et al. [31] showed the effect of variable thickness on the boundary layer over a continuously stretching sheet with power surface velocity. Elbashbeshy et al. [32] studied the flow and heat transfer over a moving surface with variable thickness in a nanofluid in the presence of thermal radiation. The study showed that increasing the power index decreases the velocity in the boundary layer near the surface, then returns to increasing it.

The present study concerns the steady flow of Maxwell nanofluid over a stretching surface. The effects of variable thickness, the porous medium, and the presence of a heat source are investigated. The model is manipulated numerically to generate the desired solutions. Important data for the modified skin friction and the modified Nusselt number are tabulated. Graphically and numerically, the effects of variable thickness, heat generation/absorption, and medium porosity on the dimensionless velocity, temperature, and concentration of the nanofluid are discussed.

2. Mathematical Formulation

Consider an incompressible, viscous, and steady-state flow of non-Newtonian Maxwell nanofluid over a two-dimensional boundary stretching surface with variable thickness as shown

in Figure 1a. The surface thickness is changed according to the surface profile $y = a(x+b)^{(1-n)/2}$ where a is a very small constant, n is power index, and b is shift constant. The surface is stretched with a variable velocity takes the form $U_w = a(x+b)^n$. Figure 1b shows the coordinate axes for the problem where x-axis is taken along the longitudinal of the stretched surface and y-axis is normal to it. The surface is impermeable. By applying the above assumptions, the governing equations are

$$\frac{\partial u}{\partial x} + \frac{\partial v}{\partial y} = 0 \tag{1}$$

$$u\frac{\partial u}{\partial x} + v\frac{\partial u}{\partial y} + \lambda_1\left[u^2\left(\frac{\partial^2 u}{\partial x^2}\right) + v^2\left(\frac{\partial^2 u}{\partial y^2}\right) + 2uv\left(\frac{\partial^2 u}{\partial x \partial y}\right)\right] = \nu\frac{\partial^2 u}{\partial y^2} - \frac{\nu}{K}u \tag{2}$$

$$\rho C_p\left(u\frac{\partial T}{\partial x} + v\frac{\partial T}{\partial y}\right) = \frac{\partial}{\partial y}\left(k\frac{\partial T}{\partial y}\right) - Q(x)(T - T_w) + \rho C_p\tau\left[D_B\frac{\partial C}{\partial y}\frac{\partial T}{\partial y} + D_B\frac{\partial C}{\partial y} + \frac{D_t}{T_\infty}\left(\frac{\partial T}{\partial y}\right)^2\right] \tag{3}$$

$$u\frac{\partial C}{\partial x} + v\frac{\partial C}{\partial y} = D_B\frac{\partial^2 C}{\partial y^2} + \frac{D_t}{T_\infty}\frac{\partial^2 T}{\partial y^2} \tag{4}$$

Equation (1) introduces the continuity equation where u and v are x and y-components of the velocity, respectively. Equation (2) is the x-momentum equation where λ_1 is the relaxation time of the fluid, ν is the kinematic viscosity of the fluid, and K is the permeability of porous medium. The temperature of the fluid is controlled by the energy equation (3) where $\tau = (\rho C)_p/(\rho C)_f$ is the ratio between the effective capacity of the nanoparticle material and the heat capacity of the fluid and C_p is the specific heat at constant pressure. The variable heat generation is $Q(x) = Q_0(x+b)^{n-1}$.

As assumed by Sulochana and Sandeep [12], the variable permeability of the porous medium is $K = K_o(x+b)^{1-n}$, and the variable density is $\rho = \rho_o(x+b)^{1-n}$ The constant surface temperature of the wall is T_w and the ambient temperature is T_∞. The rescaled nanoparticle volume fraction C is controlled by the nanoparticle equation (4). The Brownian diffusion coefficient is D_B and the thermophoresis diffusion coefficient is D_t.

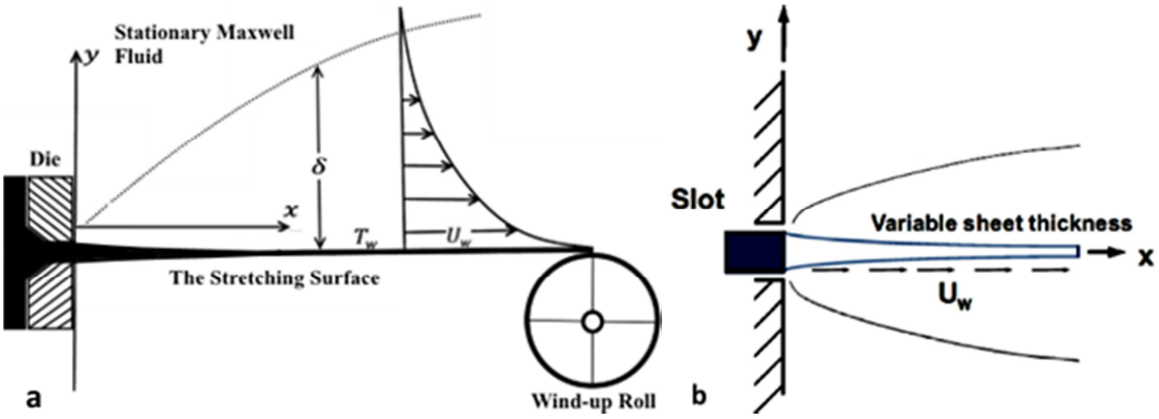

Figure 1. Schematic for flow above stretching surface.

The previous equations are subject to the boundary conditions

$$\begin{gathered} at\ y = \mathrm{a}(x+b)^{\frac{1-n}{2}}: u = U_w = \mathrm{a}(x+b)^n, v = 0, T = T_w, D_B\frac{\partial C}{\partial y} + D_t\frac{\partial T}{\partial y} = 0 \\ as\ y \to \infty: u \to 0, T \to T_\infty, C \to C_\infty \end{gathered} \tag{5}$$

As suggested in [32-34], the dimensionless similarity variables

$$\xi = \sqrt{\left(\frac{n+1}{2}\right)\frac{\mathrm{a}(x+b)^{n-1}}{\nu}}\,y;\ \psi = \sqrt{\frac{2}{n+1}\nu\mathrm{a}(x+b)^{n+1}}\,F(\xi); \theta(\xi) = \frac{T-T_w}{T_w-T_\infty};\ \varphi(\xi) = \frac{C-C_\infty}{C_W-C_\infty} \tag{6}$$

are used to simplify the governing equations where ξ is a dimensionless coordinate and ψ is the stream function. The dimensionless functions are f, θ and φ used to convert the partial differential equations into nonlinear ordinary differential equations where $\alpha = a\sqrt{a(n+1)/2\nu}$ is the wall thickness parameter used to describe the wall profile of the stretched surface. The continuity equation (1) is satisfied by assuming that

$$u = \frac{\partial \psi}{\partial y}, v = -\frac{\partial \psi}{\partial x} \tag{7}$$

Upon using equations (5-7), the governing equations (2-4) are reduced into the dimensionless form of nonlinear ordinary differential equations

$$F''' + FF'' - \frac{2n}{n+1}F'^2 + \beta\left((3n-1)FF'F'' - \frac{2n(n-1)}{n+1}F'^3 + \frac{n-1}{2}\eta F'^2F'' - \frac{n+1}{2}F^2F'''\right) - \lambda F' = 0 \quad (8)$$

$$\left(\frac{2n}{n+1}\right)F'\theta - F\theta' = \left(\frac{1}{Pr}\right)[\theta''] + \gamma\theta + N_b\theta'\phi' + N_t\theta'^2 = 0 \quad (9)$$

$$\phi'' + \frac{N_t}{N_b}\theta'' = Le\left[\left(\frac{2n}{n+1}\right)F'\phi - f\phi'\right] \quad (10)$$

subject to the dimensionless boundary conditions

$$F(\alpha) = \alpha\left(\frac{1-n}{1+n}\right), F'(\alpha) = 1, \theta(\alpha) = 1, N_b\phi'(\alpha) + N_t\theta'(\alpha) = 0,$$
$$\lim_{\eta\to\infty} F'(\eta) = 0, \lim_{\eta\to\infty}\theta(\eta) = 0, \lim_{\eta\to\infty}\phi(\eta) = 0 \quad (11)$$

where $\beta = \lambda_1 a(x+b)^{n-1}$ is the elasticity number Hayat [34], $\lambda = 2v/ak_o(n+1)$ is the porosity parameter, $Pr = \mu C_p/k_\infty$ is the Prandtl number, $\gamma = 2Q_o/\rho_o C_p a(n+1)$ is the heat generation ($\gamma > 0$) and absorption ($\gamma < 0$) parameter, the Brownian motion is $N_b = a(\tau D_B/v)(x+b)^n$, the thermophoresis parameter is $N_t = (a\tau D_t/T_\infty v)(x+b)^n$, and the Lewis number is $Le = (v/D_B)$. Let $F(\xi) = f(\xi-\alpha) = f(\eta)$, $\theta(\xi) = \theta(\xi-\alpha) = \theta(\eta)$, and $\phi(\xi) = \phi(\xi-\alpha) = \phi(\eta)$ Therefore, the similarity equations (8) to (10) in combined with the boundary conditions (11) become

$$f''' + ff'' - \frac{2n}{n+1}f'^2 + \beta\left((3n-1)ff'f'' - \frac{2n(n-1)}{n+1}f'^3 + \frac{n-1}{2}\eta f'^2f'' - \frac{n+1}{2}f^2f'''\right) - \lambda f' = 0 \quad (12)$$

$$\left(\frac{2n}{n+1}\right)f'\theta - f\theta' = \left(\frac{1}{Pr}\right)[\theta''] + \gamma\theta + N_b\theta'\phi' + N_t\theta'^2 = 0 \quad (13)$$

$$\phi'' + \frac{N_t}{N_b}\theta'' = Le\left[\left(\frac{2n}{n+1}\right)f'\phi - f\phi'\right] \quad (14)$$

subject to the dimensionless boundary conditions

$$f(0) = \alpha\left(\frac{1-n}{1+n}\right), f'(0) = 1, \theta(0) = 1, N_b\phi'(0) + N_t\theta'(0) = 0,$$
$$\lim_{\eta\to\infty} f'(\eta) = 0, \lim_{\eta\to\infty}\theta(\eta) = 0, \lim_{\eta\to\infty}\phi(\eta) = 0 \quad (15)$$

the local skin friction C_{fx}, the Nusselt number Nu_x, and Sherwood number Sh_x are important physical quantities which are defined as

$$C_{fx} = -\frac{\mu_f}{\rho U_w^2}\left(\frac{\partial u}{\partial y}\right)_{y=0}, Nu_x = \frac{xq_w}{k(T_w - T_\infty)}, Sh_x = \frac{xq_m}{D_B(C_w - C_\infty)} \quad (16)$$

where k is the thermal conductivity of the nanofluid and q_w and q_m are the heat and mass fluxes at the surface Mabood et al. [13], respectively; given by

$$q_w = -\left(\frac{\partial T}{\partial y}\right)_{y=0}, q_m = -D_B\left(\frac{\partial x}{\partial y}\right)_{y=0} \quad (17)$$

using the similarity transformation, equation (17) takes the following form

$$C_{fx}\sqrt{Re_x} = -2\sqrt{\frac{n+1}{2}}f''(0), \frac{Nu}{\sqrt{Re_x}} = -\sqrt{\frac{n+1}{2}}\theta'(0), \frac{Sh_x}{\sqrt{Re_x}} = -\sqrt{\frac{n+1}{2}}\phi'(0) \quad (18)$$

3. Results and Discussion

The nonlinear differential equations (12-14) subjected to the boundary conditions equation (15) are solved numerically using the shooting method with fourth/fifth order Runge-Kutta method used and detailed by Elbashbeshy et al. [35]. A comparison between the results of $-f''(0)$ in this study and the corresponding results in [30, 31] is tabulated in Table 1. Table 2 presents a comparison between the results of $-\theta'(0)$ with previous results given in [13, 36, 37, 38] when $n = 1$ (flat surface) and $\gamma = 0$.

Table 1 discloses that the present numerical results for the local skin friction $-f''(0)$ at different values of α (neglecting the effect of the porous medium $\lambda = 0$ and the Maxwell effect

$\beta = 0$) show an excellent agreement with the results given in [30, 31] at different values of n. Table 2 displays an excellent agreement with the previously published results. Thus, Tables 1 and 2 guarantee the numerical scheme used in this study.

Table 1. A comparison with others for $-f''(0)$ for values of α and n at $\lambda = \beta = 0$.

n	$\alpha = 0.25$			$\alpha = 0.5$		
	T. Fang [31]	Khader et al. [30]	Present Work	T. Fang [31]	Khader et al. [30]	Present Work
10	1.1433	1.1433	1.14332	1.0603	1.0603	1.06032
9	1.1404	1.1404	1.14039	1.0589	1.0588	1.05891
7	1.1323	1.1322	1.13228	1.0550	1.0551	1.05504
5	1.1186	1.1186	1.11859	1.0486	1.0486	1.04861
3	1.0905	1.0904	1.09049	1.0359	1.0358	1.03586
1	1.0000	1.0000	1.00000	1.0000	1.0000	1.00000
0.5	0.9338	0.9337	0.93382	0.9799	0.9798	0.97994
0	0.78439	0.7843	0.78427	0.9576	0.9577	0.95764
-1/3	0.5000	0.5000	0.50000	1.0000	1.0000	1.00000
-0.5	0.0833	0.0832	0.08333	1.1667	1.1666	1.16666

Table 2. Comparison of $-\theta'(0)$ for various values of Pr at $\alpha = \beta = \gamma = \varepsilon = \lambda = 0$ and $n = 1$.

Pr	Salahuddin et al. [36]	Kan and Bop [38]	Mabood et al. [13]	Wang [37]	Present Work
0.07	0.0654	0.0663	0.0655	0.0656	0.06520
0.20	0.1688	0.1691	0.1691	0.1691	0.16908
0.7	0.4534	0.4539	0.4539	0.4539	0.45391
2.00	0.9108	0.9113	0.9114	0.9114	0.91135
7.00	1.8944	1.8954	1.8954	1.8954	1.89540
20.00	3.3522	3.3539	3.3539	3.3539	3.35390
70.00	6.4619	6.4621	6.4622	6.4622	6.46219

Figures 2-21 show the influences of wall thickness, elasticity, porosity, heat generation/absorption, Brownian, and thermophoresis parameters and Prandtl and Lewis numbers on the velocity, temperature, and nanoparticle concentration profiles for the boundary layer flow of the nanofluids

3.1. The Index Power n

The surface profile of the stretching surface (see Figure 1b) is described according to the index power n. Increasing the value for n leads to a greater decreases in the surface thickness. Also, the index power n describes the stretching wall velocity U_w. The effects of this parameter on the dimensionless velocity, temperature, and concentration are illustrated in Figures 2-4, respectively, for $n = 0, 0.5, 3$ at $\alpha = 0.25, \beta = 0.6, \gamma = 0.1, -0.1, \varepsilon = 0.1, \lambda = 0, 0.2$, $Pr = 1, Nt = Nb = 0.2$ and $Le = 1, 3$.

It is important to denote that the dimensionless velocity f' represents the ratio of the fluid velocity component u to the stretching velocity U_w. For that, increasing the velocity index power n means an increase in the stretching surface velocity and the curvature of the profile surface. Consequentially, it causes a decrease in the dimensionless velocity as shown in Figure 2, and so a decrease in the momentum boundary layer.

In the same figure, the influence of the porosity parameter λ takes place where this parameter is a measurement for the ease of the fluid to penetrate through a porous medium. Due to this fact, the increase in this parameter increases the resistive force to inhibit the nanofluid to flow through the porous medium. Figure 2 ensures this fact where the existence of a porous medium causes a decrease in the dimensionless velocity f'. Figure 3 shows a increase in the dimensionless temperature θ and the existence of heat source encourages this increase.

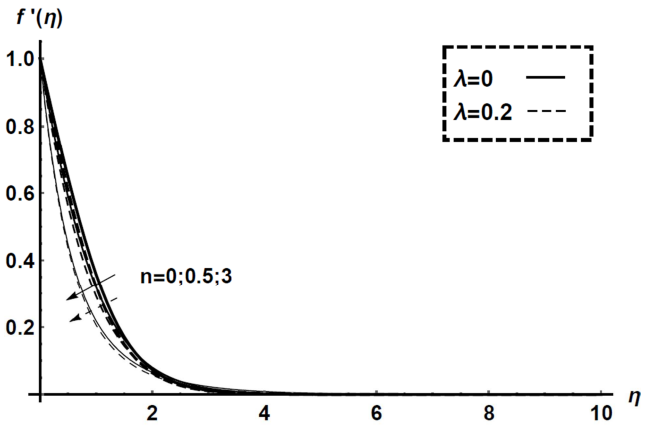

Figure 2. Effects of n on dimensionless velocity at $\alpha = 0.25$ and $\beta = 0.6$.

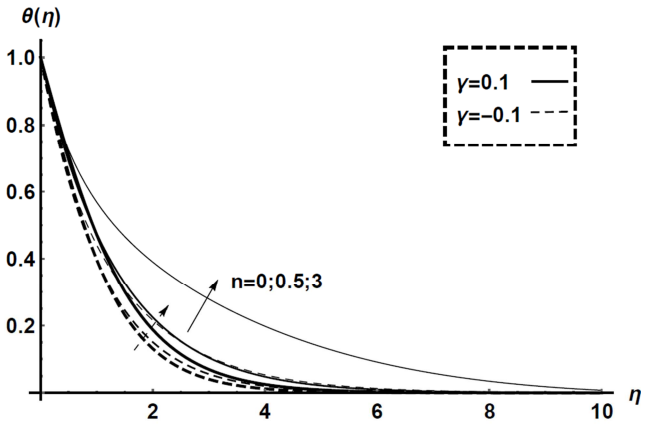

Figure 3. Effects of n on dimensionless Temperature at $\alpha = 0.25$, $\beta = 0.6$, and $Pr = 1$.

Figure 4 shows that the dimensionless concentration decreases with n due to increases in the reference concentration $C_w - C_\infty$. In the same figure, the influence of Lewis number $Le = (v/D_B)$ is presented. This parameter is a dimensionless number presenting the ratio of the thermal diffusivity to the mass diffusivity. This number is taken as a characterization of the fluid flows. The increase in this number means that the diffusion of the heat is higher than the mass diffusivity so the fluid concentration is decreased due to the increase in Le number.

3.2. Wall Thickness Parameter α

The effect of wall thickness parameter $\alpha = A\sqrt{a(n+1)/2v}$ on the velocity, temperature, and dimensionless concentration profiles are shown in Figures 5-10, respectively, for $\alpha = 0.1, 0.8, 1.2$ at $n = 0.5, 1.2$, $\beta = 0.6$, $\gamma = 0.1, -0.1$, $\varepsilon = 0.1$, $\lambda = 0, 0.2$, $Pr = 1, Nt = Nb = 0.2$, and $Le = 1, 3$.

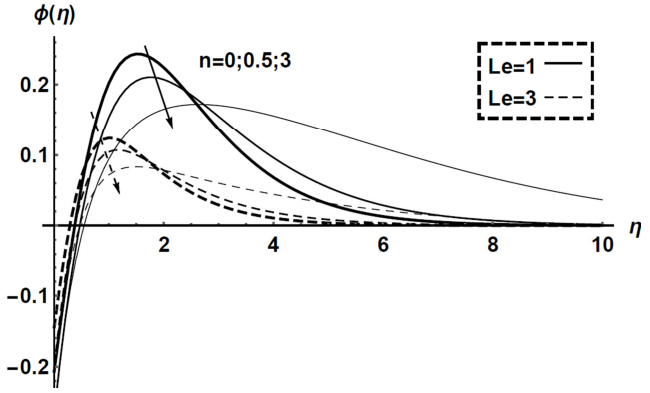

Figure 4. Effects of n on dimensionless concentration at $Nt = Nb = 0.2$, $\alpha = 0.25$ and $\beta = 0.6$.

Figure 5a illustrates that the wall thickness parameter causes a decrease in the velocity and consequentially the boundary layer thickness becomes thinner for $n < 1$. This effect is revert for $n > 1$ as shown in Figure 5b and the boundary layer thickness becomes thicker. The porosity parameter in the two previous cases encourages the effect of α on the dimensionless velocity.

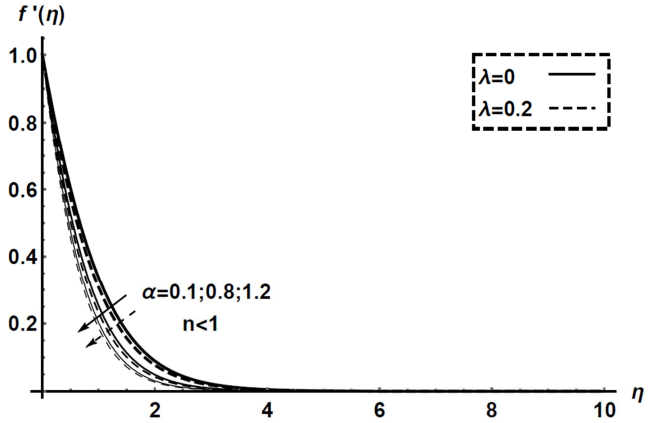

Figure 5a. Effects of α on dimensionless velocity at $n = 0.5$ and $\beta = 0.6$.

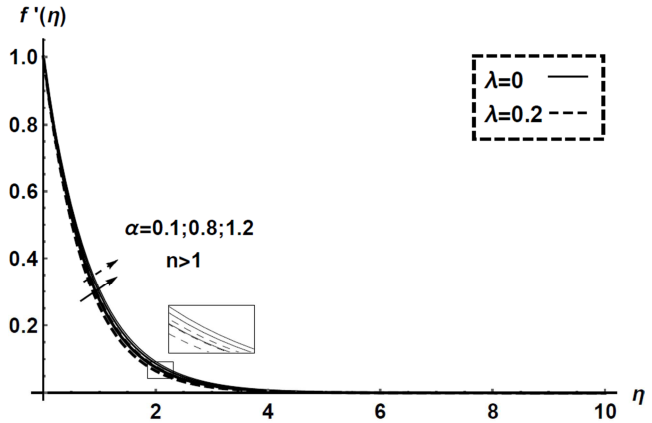

Figure 5b. Effects of α on dimensionless concentration at $n = 1.2$ and $\beta = 0.6$.

Figure 6a displays that the dimensionless temperature decreases for the high values of α at $n < 1$, and it increases at $n > 1$ as shown in Figure 6b. The existence of heat generation source encourages this phenomenon. Figure 7a shows an increase in the dimensionless concentration with α at $n < 1$ and Figure 7b shows a decrease at $n < 1$, also increasing Lewis number encourages the effect of α on the concentration.

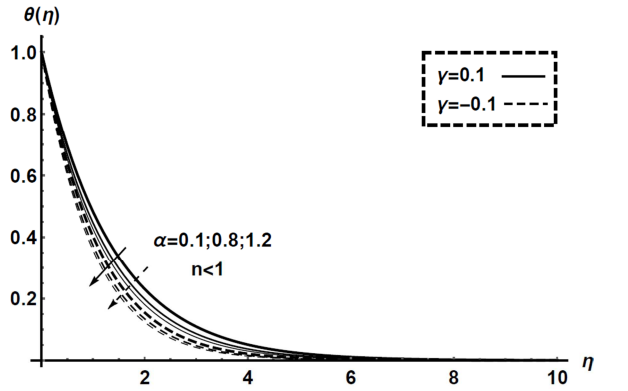

Figure 6a. Effects of α on dimensionless Temperature at $n = 1.2$, $Pr = 1$, $\varepsilon = 0.1$ and $\beta = 0.6$.

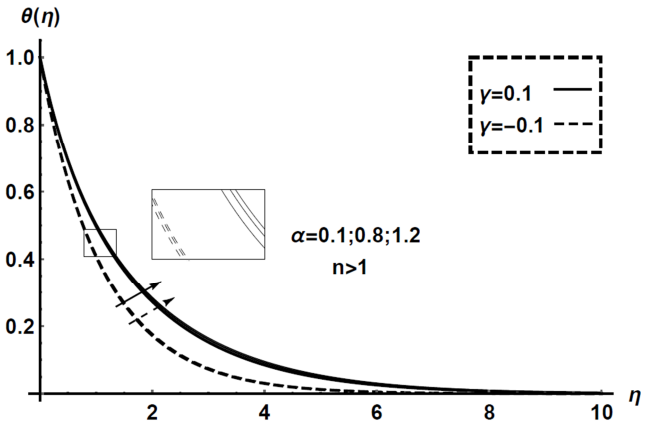

Figure 6b. Effects of α on dimensionless temperature at $n = 1.2$, $Pr = 1$, $\varepsilon = 0.1$ and $\beta = 0.6$.

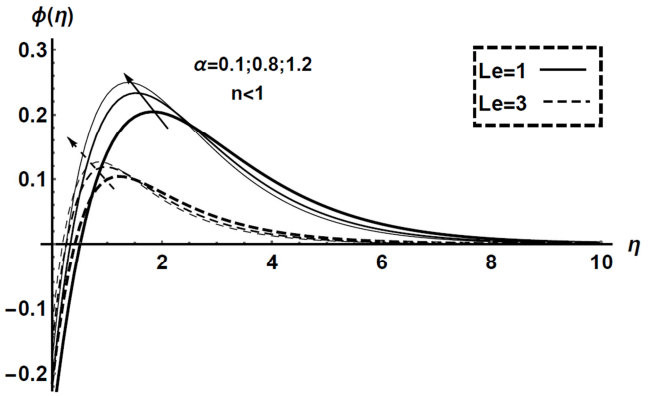

Figure 7a. Effects of α on dimensionless concentration at $n = 0.5$ and $Nt = Nb = 0.2$.

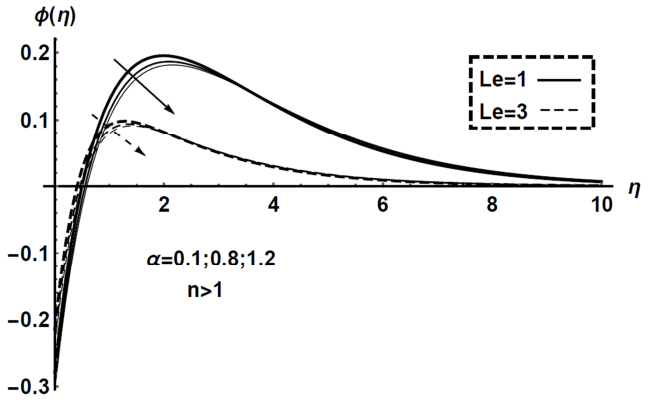

Figure 7b. Effects of α on dimensionless concentration at $n = 1.2$ and $Nt = Nb = 0.2$.

3.3. Elasticity Parameter β

The elasticity parameter β of Deborah number is a dimensionless number represents the ratio of the time scale flow to the relaxation time flow. Where, the time scale is used to distinguish the type of the unsteady flow. For instant, when the time scale approaches infinity, the flow becomes steady and the relaxation time is the time required to the viscous fluid to retain after the flow stopped due to the effect of shear stress. The effect of the elasticity parameter on the dimensionless velocity, temperature and concentration are shown in the Figures. 11 to 13 respectively for $\beta = 0, 0.5, 1$ at $n = 0.5$, $\alpha = 0.25$, $\gamma = 0.1, -0.1$, $\varepsilon = 0.1$, $\lambda = 0, 0.2$, $Pr = 1$, $Nt = Nb = 0.2$ and $Le = 1, 3$. Figure 8 shows a decrease in the velocity while an increasing in the elasticity number. This is due to the fact that increasingly β makes the fluid more viscous and so the resistance within the fluid is increased and the porous medium increases this resistance. This fact increases the temperature as shown in Figure 9 and the existence of heat source encourages that, and it increases the concentration too as shown in Figure 10 and the thermophoresis parameter enhances that.

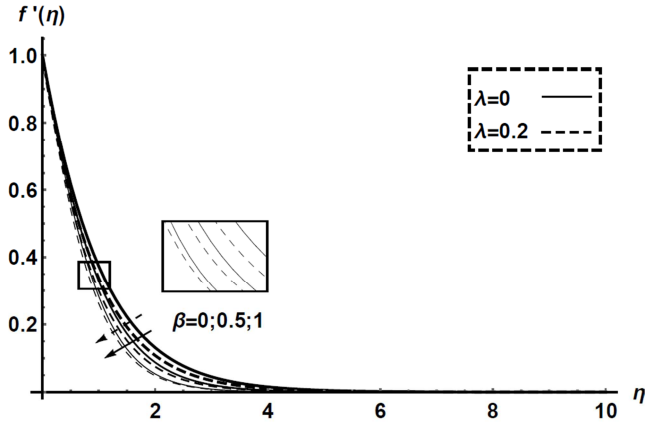

Figure 8. Effects of β on dimensionless velocity at $n = 0.5, \alpha = 0.25$.

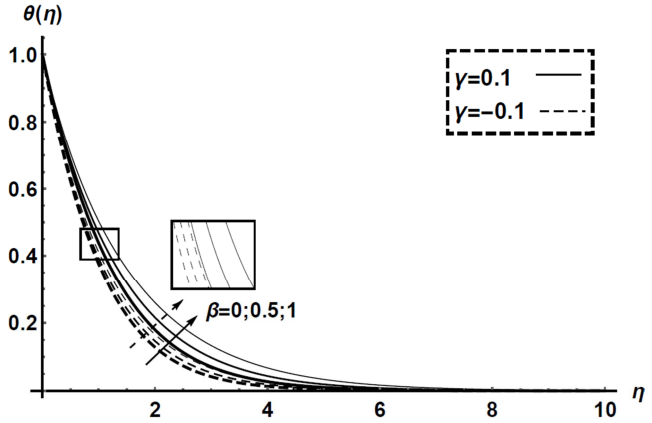

Figure 9. Effects of β dimensionless temperature at $n = 0.5, \alpha = 0.25, \varepsilon = 0.1$ and $Pr = 1$.

3.4. Porosity Parameter λ

The fluid combined with the nanoparticles is considered as a porous medium. The porosity parameter λ is used to detect the level of porosity for these fluids. This parameter increases the effect of the free stream velocity in comparison with the stretching velocity, which results in the increase in the pressure. The effects of this parameter on dimensionless velocity, temperature and concentration are shown in the Figures 11-13 respectively, for $\lambda = 0, 0.5, 1$ at $n = 0.5$, $\alpha = 0.25$, $\beta = 0.6, \gamma = 0.1, -0.1$, $\varepsilon = 0.1, Pr = 1$, $Nt =$

$Nb = 0.2$ and $Le = 1, 3$. Figure 11 shows a decrease in the dimensionless velocity and consequentially the boundary layer becomes thinner for the non-Newtonian fluid ($\beta = 0.6$) than for Newtonian one ($\beta = 0$) with increasing the porosity parameter, while the dimensionless temperature increases as shown in Figure 12 and the existence of the heat source encourages this effect. Figure 13 shows an increase in the concentration with increasing the porous parameter and Lewis number.

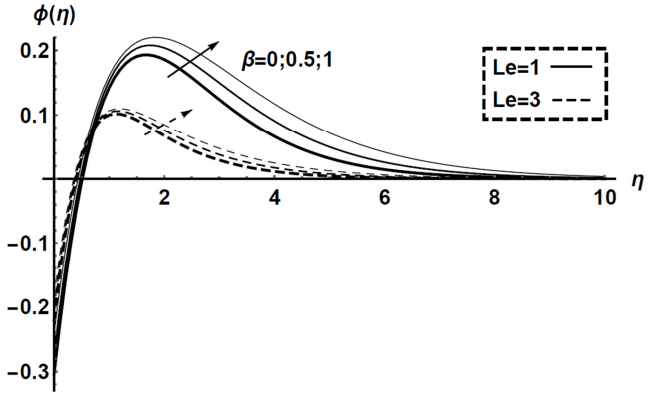

Figure 10. Effects of β on dimensionless concentration at $n = 0.5, \alpha = 0.25$ and $Nb = Nt = 0.2$.

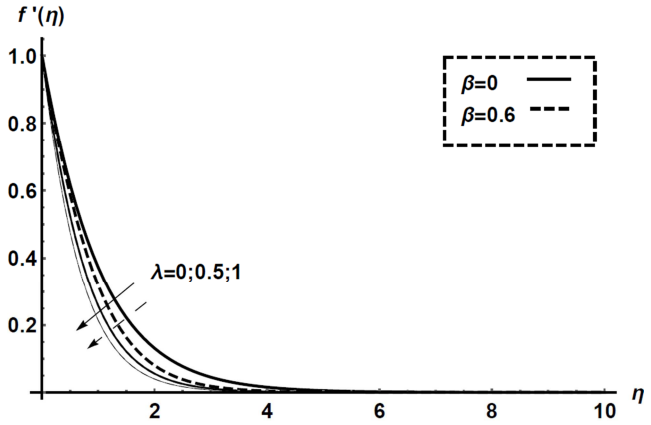

Figure 11. Effects of λ onn dimensionless velocity at $n = 0.5$ and $\alpha = 0.25$.

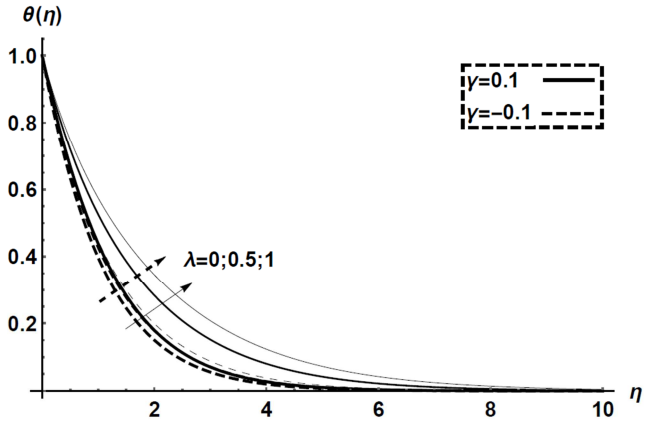

Figure 12. Effects of λ on dimensionless temperature at $n = 0.5, \alpha = 0.25, \beta = 0.6, \varepsilon = 0.1$ and $Pr = 1$.

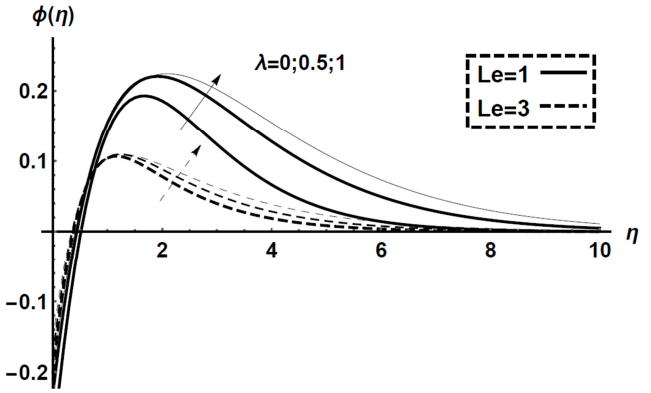

Figure 13. Effects of λ on dimensionless concentration at $n = 0.5, \alpha = 0.25, \beta = 0.6$ and $Nt = Nb = 0.2$.

3.5. Internal Heat Source/Sink

The existence of internal heat source/sink is declared using the heat generation/absorption parameter. The effect of this parameter is shown in the Figures 14-15 respectively, for $\gamma = -1, 0, 1$ at $n = 0.5$, $\alpha = 0.25, \beta = 0.6, \varepsilon = 0.1, Pr = 1$, $Nt = Nb = 0.2$, and $Le = 1, 3$.

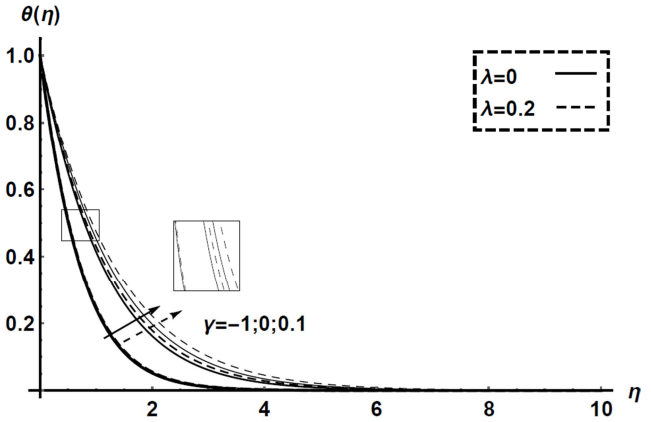

Figure 14. Effects of γ on dimensionless velocity at $n = 0.5$, $\alpha = 0.25$ and $\beta = 0.6$.

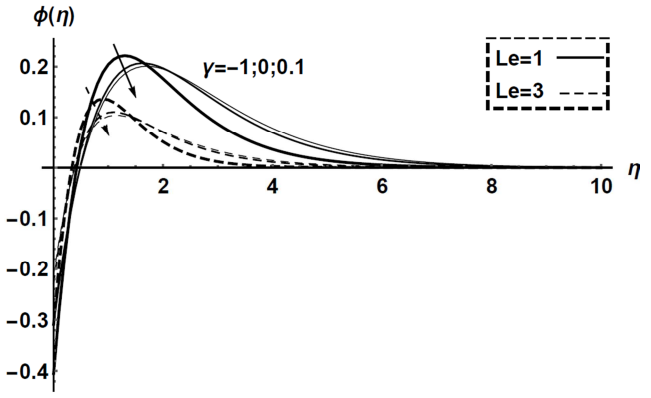

Figure 15. Effects of γ and Le on dimensionless concentration at $n = 0.5$, $\alpha = 0.25$ and $\beta = 0.6$.

Figure 14 shows that the dimensionless temperature increases with the existence of the heat source and the porous medium enhances this effect. Figure 18 shows that the dimensionless

concentration decreases, and increasing the Lewis number enhances the effect of the heat source.

3.6. Prandtl Number Pr

Prandtl number Pr introduces the ratio between the momentum diffusivity and the thermal diffusivity. The effect of this parameter on the dimensionless temperature and concentration profiles are shown in Figures 16-17 respectively, for $Pr = 0.7,1,3$ at $n = 0.5$, $\alpha = 0.25, \beta = 0.6, \varepsilon = 0.1, \gamma = 0.1, -0.11, Nt = Nb = 0.2$ and $Le = 1,3$.

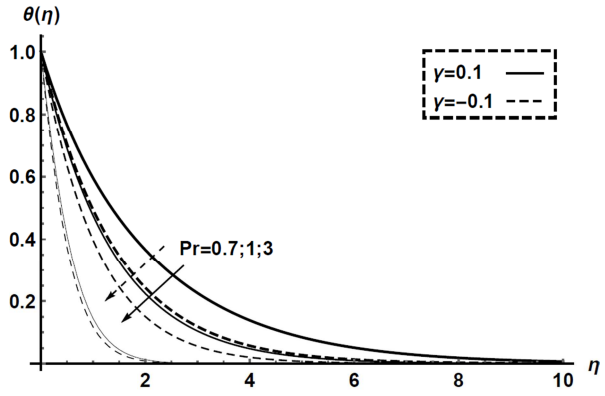

Figure 16a. Effects of Pr on dimensionless temperature.

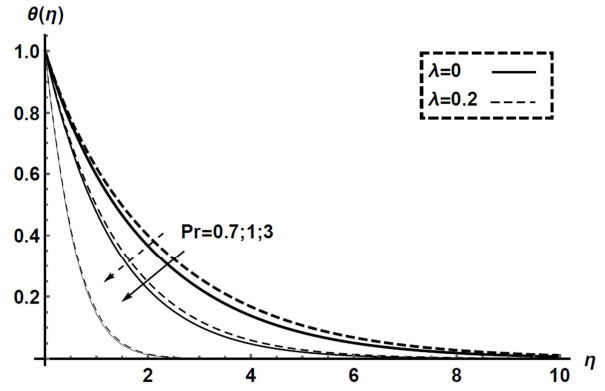

Figure 16b. Effects of Pr on dimensionless temperature.

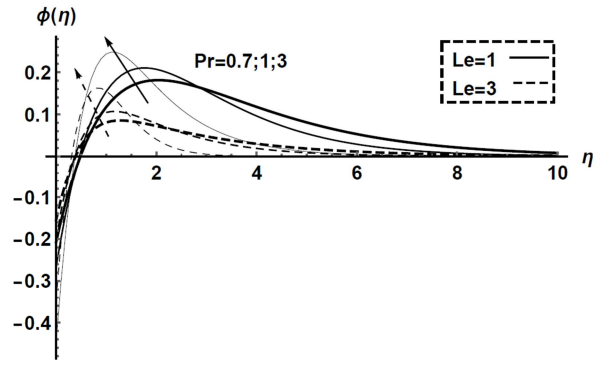

Figure 17. Effects of Pr and Le on dimensionless concentration.

Figure 16 shows a decrease in the temperature with increasing Prandtl number. Physically, increasing Prandtl number means that the momentum diffusivity increases and the thermal diffusivity decrease. The existence of heat source encourages the effect of Pr number as shown in Figure 16a, also the existence of porous medium as shown in Figure 16b. Figure 17 shows an increase in the dimensionless concentration while increasing Prandtl number and Lewis number.

3.7. Lewis Number Le

For the high values of Lewis number, the effect of mass diffusion takes place inducing a raise in the dimensionless concentration as shown in Fig 18. The existence of porous medium slightly increases this effect as shown in Figure 18a, and the existence of heat generation source decreases the dimensionless concentration as shown in Figure 18b.

3.8. Thermophoresis Parameter Nt

As previously mentioned, Nanoparticles are mixture of different types of materials with different response to the thermal gradient. This difference in response creates an internal force called thermophoresis force. This force creates a fast flow away from the stretching surface, so it moves the heat away from the surface. This movement increases the temperature in the boundary layer as shown in Figure 19. The existence of heat source encourages the Nt effect as shown in Figure 19a and the existence of porous medium encourages the Nt effect too as shown in Figure 19b.

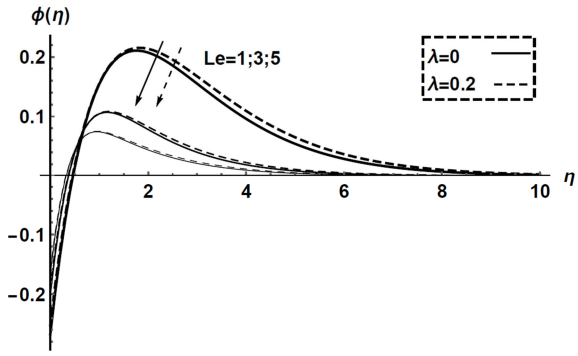

Figure 18a. Effects of Le and λ on dimensionless temperature.

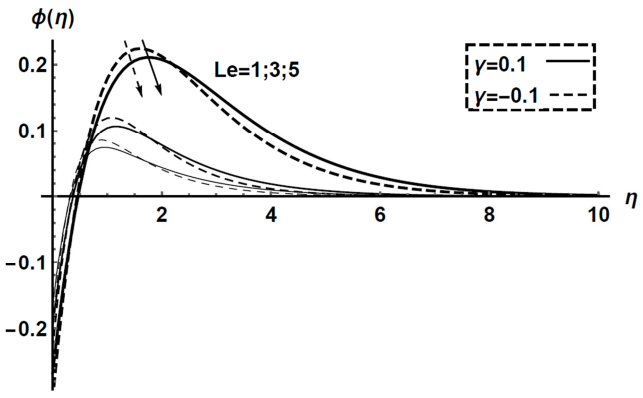

Figure 18b. Effects of Le and γ on dimensionless concentration.

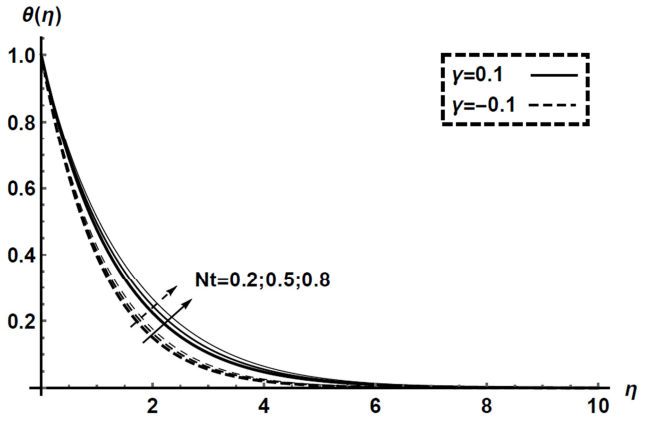

Figure 19a. Effects of Nt on dimensionless temperature.

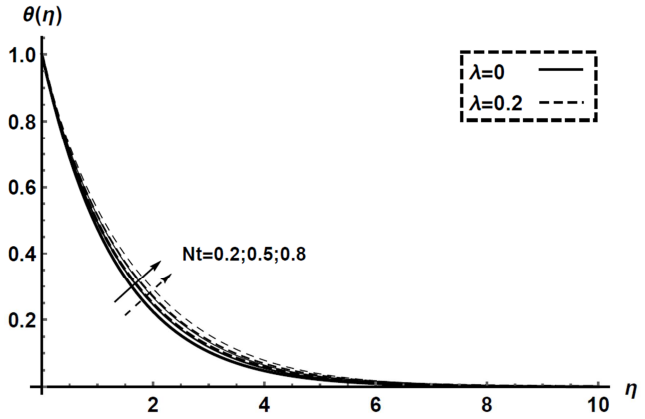

Figure 19b. Effects of Nt on dimensionless temperature.

Figure 20 shows an increase in the dimensionless concentration while increasing the thermophoresis parameter and the Lewis number.

3.9. Brownian Parameter NB

The random collision of the nanoparticle with the fast particles in the base fluid called the Brownian diffusion. At the high values of Brownian parameter, the random diffusion is high, so the dimensionless concentration decreases as shown in Figure 21 and the Lewis number enhances this effect.

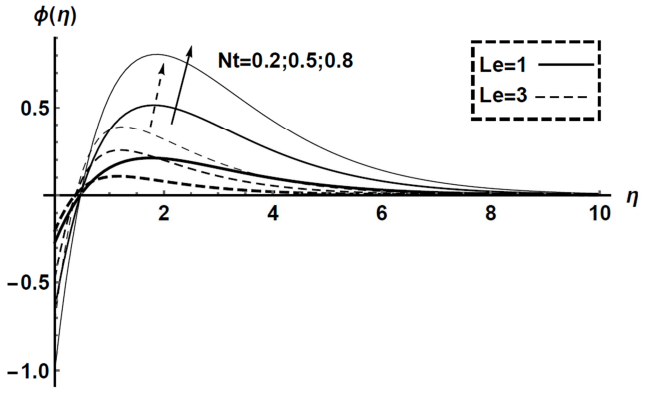

Figure 20. Effects of Nt on dimensionless concentration.

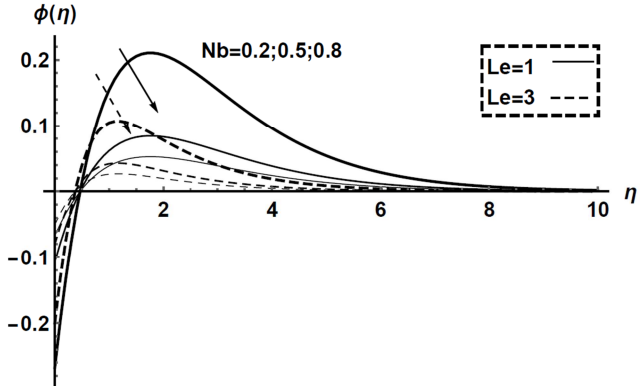

Figure 21. Effects of N_B and Le on dimensionless velocity.

By introducing Figure 21, the graphical presentation for the influence of different parameters on the Nanofluid flow over a stretched surface with variable thickness is ended. In the next section, important quantities for the flow will be discussed such as the local skin friction, the local Nusselt number…etc.

3.10. Modified Skin-Friction and Modified Nusselt Number

The ratio of the inertial force to the viscous force in a fluid is defined as dimensionless number called Reynold number. This number defines the flow type to be laminar, transient, or turbulent. The friction force between the stretching surface and the adjacent fluid particles called skin-friction. This friction creates a drag force depending on the value of Reynold number and takes different values depending on the local value of the Reynold number, so it is called the modified skin-friction. The modified Nusselt number is another dimensionless number defines the ratio of the convective heat transfer to the conduction one.

Table 3. Introduces a tabulated data for the modified local skin-friction and the local Nusselt number at different settings.

n	α	β	λ	Pr	γ	$C_{fx}\sqrt{Re_x}$L	$Nu/\sqrt{Re_x}$
0.5	0.25	0.6	0.2	1	0.1	1.851147	0.609477
1						2.4654	0.573017
3						4.716487	0.523854
0.5	0.2	0.6	0.2	1	0.1	1.82475	0.591484
0.5	0.5					1.992707	0.699852
3	0.2					4.855617	0.609996
3	0.5					4.09873	0.724371
0.5	0.25	0	0	1	0.1	1.617432	0.666275
		0.5				1.668365	0.570444
		1				1.729624	0.540324
0.5	0.25	0.6	0	1	0.1	1.679878	0.631433
			0.5			2.084939	0.516896
			1			2.427798	0.472011
0.5	0.2	0.6	0.2	0.7	0.1	1.851147	0.447261
				1		1.851147	0.545133
				3		1.851147	1.180246
0.5	0.25	0.6	0.2	1	-1	1.851147	2.011762
					0	1.851147	1.253007
					0.1	1.851147	0.545133

The first part in Tab. 3 shows that the modified skin friction increases while and the modified Nusselt numbers decreases with increasing the velocity power index. Physically, increasing the power index n increases the effect of the friction between the surface and the adjacent fluid, and increases the heat transfer by conduction. The second part in Tab. 3 shows that increasing the wall thickness parameter α for convex outer shape ($n < 1$) increases the modified skin-friction and Nusselt number while for concave outer surface ($n > 1$) it decreases only the modified skin friction, which indicates that the effect of the wall thickness parameter is mainly effected by the surface outer shape.

As mentioned before, for high β, the viscosity and resistivity of the fluid are increased inducing more friction within the fluid and reduces the velocity of the flow. These effects appear in the increasing of the modified skin friction and lowering of the modified Nusselt number as tabulated in the third part of Table 3. The fourth part of Tab. 3 indicates the increase in the modified skin friction and decreasing in the modified Nusselt number with the porous parameter. The fifth and six parts of Tab. 3 show the effect of Prandtl number and the internal heat source, respectively. For high Prandtl numbers, the modified Nusselt number is high. Also, the existence of heat source increases the modified Nusselt number. The two parameters have no effect on the local skin-friction.

Table 4. The Sherwood number.

n	N_t	N_B	$Sh_x/\sqrt{Re_x}$
0.2	0.2	0.2	0.530854
0.5	0.2	0.2	0.673189
0.7	0.2	0.2	0.7479811
1	0.2	0.2	0.305205
3	0.2	0.2	0.50852071
4	0.2	0.2	0.5454763
1	0.2	0.1	0.70484
1	0.2	0.3	0.23494
1	0.2	0.5	0.14096
1	0.1	0.2	0.17884
1	0.3	0.2	0.52076
1	0.5	0.2	0.84192

3.11. Sherwood Number

Sherwood number presents the ratio of the mass transferred by convection to the mass transferred by diffusion. This number is expressed as a function of Reynold and Schmidt numbers. Table 4 introduces the effect of the Brownian motion and the thermophoresis parameter on Sherwood number for different values of N_t and N_B at $Pr = Le = 2$, $\lambda = 0.2$, $\alpha = 0.25$, β=0.6, and $\gamma = 0.1$. For $Nt = Nb = 02$. The first part of Table 4 shows that Sherwood number increases for $n < 1$, while for $n = 1$, it takes its lowest value. For $n > 1$, it continues its increasing again. This all explains the effect of the surface profile and the stretching velocity on the mass transfer. The second part of Table 4 shows the effect of the Brownian motion on Sherwood number for the flat surface, where Sherwood number is decreasing with increasing the Brownian parameter. Physically, increasing Brownian parameter means a lot of collisions between the fluid molecules, so the mass diffusivity increases causing a decrease in Sherwood number. Finally, the third part of Table 4 shows that the thermophoresis parameter increases the mass transferred by convection and so Sherwood number increases.

4. Conclusions

Heat and mass transfer of a Maxwell Nanofluid over a stretching surface with variable thickness embedded in porous medium have been investigated numerically. A similarity transformation for the governing boundary layer equations has been done based on wall thickness, elasticity, porosity, heat generation/absorption, Brownian and thermophoresis parameters, Prandtl and Lewis numbers. The effects of these parameters and numbers on the flow velocity, concentration and heat transfer have been presented graphically. The results for the local skin-friction, Nusselt and Sherwood numbers have been tabulated. The observations of the present study can be summarized in the following points.

a) The heat transfer increases with the increase in the index power, the wall thickness α for $n > 1$, the elasticity β, and the porosity λ parameters, and the existence of heat generation source while it decreases with the increase in Prandtl number.

b) The increase of the thermophoresis parameter improves the heat transfer, and the existence of heat source in combined with increasing the Brownian motion improves the heat transfer.

c) The nanofluid velocity decreases with the increase in the index power n, the wall thickness α for $n < 1$, the elasticity β, and the porosity λ parameters

d) The dimensionless concentration decreases with the increase in the index power, and the wall thickness α for $n > 1$ parameters while it increases with the increase in the elasticity β, the porosity λ parameters and Prandtl number Pr.

e) The Brownian motion decreases the concentration by increasing the random diffusion.

f) The increase in Lewis number reduces the effect of the previous parameters on the concentration.

g) The local skin-friction increases with the increase in the index power n and the elasticity parameter β.

h) The local Nusselt number increases with the increase in the index power n and Prandtl number Pr while it decreases with the increase in the elasticity parameter β and the heat generation source.

i) The Sherwood number increases with the increase in the index power n, and the thermophoresis parameter Nt, and it decreases with the increase in the Brownian parameter NB.

Nomenclature

a, b	Constants
C	Rescaled nanoparticle volume fraction
C_p	Specific heat at constant pressure,$J/Kg\ K$
C_f	Local skin-friction coefficient
D_B	Brownian diffusion coefficient
D_t	Thermophoresis diffusion coefficient
f, F	Dimensionless functions
k	Thermal conductivity
k_∞	ambient thermal conductivity
K	Permeability of porous medium, m^2
K_o	Reference permeability of porous medium
n	Velocity power index
N_B	The Brownian motion parameter
N_t	The thermophoresis parameter
Nu	Nusselt number
Pr	Prandtl number
Q	Rate of Heat generation/absorption
q_m	Mass flux of the nanofluid
q_w	Heat flux of the nanofluid
Sh_x	Sherwood number
Re_x	Local Reynold's number
T	The temperature, K
T_∞	Ambient temperature, K
U_w	Velocity of solid surface
u, v	Velocity components along x and y, m/s
x, y	Distance along and normal to the surface
Greek symbols	
α	Wall thickness parameter
β	The elasticity parameter
γ	Heat generation/absorption parameter
η, ξ	Dimensionless coordinate
θ, ϕ	Dimensionless temperature
λ	Porous parameter
λ_1	The relaxation time of the fluid
v	Kinematical viscosity= $\mu/\rho, m/s^2$
ρ	Fluid density, Kg/m^3
μ	Dynamical viscosity, $Kg/m.s$
ψ	Physical stream function
Subscripts	
x	Local value
w	Condition on the wall
∞	Free stream (ambient) condition
O	Reference value

References

[1] Xuan, Y. and Qiang, Li. (2000). Heat transfer enhancement of nanofluids, International Journal of Heat and Fluid Flow, vol. 21, pp. 58-64.

[2] Daungthongsuk, W. and Wongwises, S. (2007). A critical review of convective heat transfer of nanofluids, Renewable and Sustainable Energy Reviews. Vol. 11, pp. 797–817.

[3] Hamilton, R. L. and Crosser, O. K. (1962). Thermal conductivity of heterogeneous two-component systems, I& EC Fundamentals, vol. 1 (3), pp. 187-191.

[4] Stephen, U. S. Choi and Eastman, J. A. (1995). Enhancing Thermal Conductivity of Fluids with Nanoparticles, ASME International Mechanical Engineering Congress & Exposition, pp. 12-17.

[5] Eastman, J. A., Choi, S. U. S., Li, S., Yu, W., and Thompson, L. J. (2001). Anomalously increased effective thermal conductivities of ethylene glycol based nanofluids containing copper nanoparticles, Applied Physics Letters, vol. 78 (6), pp. 718-720.

[6] Xie, H., Wang, J., Xi, T., Liu, Y., and Ai, F. (2002). Thermal conductivity enhancement of suspensions containing nanosized alumina particles, Applied Physics Letters, vol. 91 (7), pp. 4568-4572.

[7] Wang, B. X., Zhou, L. P., and Peng, X. F. (2003). A fractal model for predicting the effective thermal conductivity of liquid with suspension of nanoparticles, International Journal of Heat and Mass Transfer, vol. 46, pp. 2665–2672.

[8] Wen, D. and Ding, Y. (2004). Effective Thermal Conductivity of Aqueous Suspensions of Carbon Nanotubes (Carbon Nanotube Nanofluids), Journal of Thermophysics and Heat Transfer, vol. 18 (4), pp. 481-485.

[9] Hong, TK., Yang, HS., and Choi, C. J. (2005). Study of the enhanced thermal conductivity of Fe nanofluids, journal of applied physics, vol. 97, 064311.

[10] Buongiorno, J. (2006). Convective Transport in Nanofluids, Journal of Heat Transfer, vol. 128, pp. 240-250.

[11] Makinde, O. D. and Aziz, A. (2011). Boundary-layer flow of a nanofluid past a stretching sheet with a convective boundary condition, International Journal of Thermal Sciences, vol. 50. pp. 1326-1332.

[12] Sulochana, C. and Sandeep, N. (2015). Dual Solutions for Radiative MHD Forced Convective Flow of a Nanofluid over a Slendering Stretching Sheet in Porous Medium, Journal of Naval Architecture and Marine Engineering, vol. 12, pp. 115-124.

[13] Mabood, F., Khan, W. A., and Ismail, A. I. M. (2015). MHD boundary layer flow and heat transfer of nanofluids over an on linear stretching sheet: A numerical study, Journal of Magnetism and Magnetic Materials, vol. 374, pp. 569–576.

[14] Elbashbeshy, E. M. A., Emam, T. G., El-Azab, M. S., and Abdelgaber, K. M. (2016). Slip Effects on Flow, Heat, and Mass Transfer of Nanofluid over Stretching Horizontal Cylinder in the Presence of Suction/Injection, Thermal Science, vol. 20, No. 6, pp. 1813-1824.

[15] Elbashbeshy, E. M. A., Asker, H. G., and Abdelgaber, K. M. (2017). Unsteady Flow of Micropolar Maxwell Fluid over Stretching Surface in The Presence of Magnetic Field, International Journal of Electronic Engineering and Computer Science, vol. 2, No 4, pp. 28-34.

[16] Sandeep, N., Sulochana, C., and Rushi Kumar, B. (2016). Unsteady MHD radiative flow and heat transfer of a dusty nanofluid over an exponentially stretching surface, Engineering Science and Technology, an International Journal, vol. 19. pp. 227-240.

[17] Pal, D. and Mandal, G. (2017). Double diffusive magnetohydrodynamic heat and mass transfer of nanofluids over a nonlinear stretching/shrinking sheet with viscous-Ohmic dissipation and thermal radiation, Propulsion and Power Research; vol. 6 (1), pp. 58-69.

[18] Sadeghy, K. and Shari, M. (2004). Local similarity solution for the flow of a "second-grade" viscoelastic fluid above a moving plate, International Journal of Non-Linear Mechanics, vol. 39, pp. 1265-1273.

[19] Aliakbar, V., Alizadeh-Pahlavan, A., and Sadeghy, K. (2009). The influence of thermal radiation on MHD flow of Maxwellian fluids above stretching sheets, Communications in Nonlinear Science and Numerical Simulation, vol. 14, pp. 779-794.

[20] Sajid, M., Ahmad, I., Hayat, T., and Ayu, M. (2009). Unsteady flow and heat transfer of a second grade fluid over a stretching sheet, Communications in Nonlinear Science and Numerical Simulation, vol. 14, pp. 96-108.

[21] Hayat T. and Qasim, M. (2010). Influence of thermal radiation and Joule heating on MHD flow of a Maxwell fluid in the presence of thermophoresis, International Journal of Heat and Mass Transfer, vol. 53, pp. 4780-4788.

[22] Mukhopadhyay, S. (2012). Heat Transfer Analysis of the Unsteady Flow of a Maxwell Fluid over a Stretching Surface in the Presence of a Heat Source/Sink, CHIN. PHYS. LETT, vol. 29, No. 5.

[23] Mukhopadhyay, S., Ranjan De, P., and Layek, G. C. (2013). Heat Transfer Characteristics for the Maxwell Fluid Flow past an Unsteady Stretching Permeable Surface embedded in a Porous Medium with thermal radiation, Journal of Applied Mechanics and Technical Physics, vol. 54, No. 3, pp. 385-396.

[24] Mukhopadhyay, S. and Bhattacharyya, K. (2012). Unsteady flow of a Maxwell fluid over a stretching surface in presence of chemical reaction, Journal of the Egyptian Mathematical Society, vol. 20, pp. 229–234.

[25] Ramesh, G. K. and Gireesha, B. J. (2014). Influence of heat source/sink on a Maxwell fluid over a stretching surface with convective boundary condition in the presence of nanoparticles, Ain Shams Engineering Journal, vol. 5, pp. 991-998.

[26] Madhua, M., Kishana, N., and J. Chamkha, A. (2017). Unsteady flow of a Maxwell nanofluid over a stretching surface in the presence of magneto hydrodynamic and thermal radiation effects, Propulsion and Power Research, vol. 6 (1). pp. 31-40.

[27] Hsiao, KL. (2017). Combined Electrical MHD Heat Transfer Thermal Extrusion System Using Maxwell Fluid with Radiative and Viscous Dissipation Effects, Applied Thermal Engineering, vol. 112, pp. 103-110. doi: 10.1016/j.applthermaleng.2016.08.208.

[28] Hsiao, KL. (2017). To Promote Radiation Electrical MHD Activation Energy Thermal Extrusion Manufacturing System Efficiency by Using Carreau-Nanofluid with Parameters Control Method, Energy, vol. 130, pp. 486-499. doi: 10.1016/j.energy.2017.05.004.

[29] Ramesh, G. K., Prasannakumara, B. C., Gireesha, B. J., and Rashidi, M. M. (2016). Casson Fluid Flow near the Stagnation Point over a Stretching Sheet with Variable Thickness and Radiation, Journal of Applied Fluid Mechanics, vol. 9 (3), pp. 1115-1122.

[30] Khader, M. M. and Megahed, A. M. (2013). Numerical solution for boundary layer flow due to a nonlinearly stretching sheet with variable thickness and slip velocity, Eur. Phys. J. Plus., pp. 128-100.

[31] Fang, T., Zhang, J., and Zhong, Y. (2012). Boundary layer flow over a stretching sheet with variable thickness, Applied Mathematics and Computation, vol. 218, pp. 7241–7252.

[32] Elbashbeshy, E. M. A., Emam, T. G., and Abdel-wahed, M. S. (2014). Flow and heat transfer over a moving surface with nonlinear velocity and variable thickness in a nanofluid in the presence of thermal radiation, Can. J. Phys., vol. 92, pp. 124-130.

[33] Hossain, M. A., Khanafer, K., and Vafai, K. (2001). The effect of radiation on free convection flow of fluid with variable viscosity from a porous vertical plate, Int. J. Therm. Sci., vol. 40, pp. 115-124.

[34] Hayat, T. Farooq, M. Alsaedi, A., and Al-Solamy, F. (2015). Impact of Cattaneo-Christov heat flux in the flow over a stretching sheet with variable thickness, AIP ADVANCES, vol. 5, 087159.

[35] Elbashbeshy, E. M. A., Emam, T. G., and Abdelgaber, K. M. (2015) Effect of Thermal Radiation on Flow, Heat, and Mass transformer of a Nanofluid Medium over A Stretching Horizontal Cylinder Embedded in a Porous Medium with Suction/Injection, Journal of Porous Media, vol. 18, No. 3.

[36] Salahuddin, T. Malik, M. Y. Hussain, A. Bilal, S., and Awais, M. (2016). MHD flow of Cattanneo–Christovheat flux modelfor Williamson fluid over a stretching sheet with variable thickness: Using numerical approach, Journal of Magnetism and Magnetic Materials, vol. 401, pp. 991–997.

[37] Wang, C. Y. (1989). Free convection on a vertical stretching surface with suction and blowing, Appl. Math. Mech., vol. 69, pp. 418–420.

[38] Khan, W. A., and Pop, I. (2010). Boundary layer flow of a nanofluid past a stretching sheet, Int. J. Heat Mass Transfer, vol. 53, pp. 2477–2483.